İlkay Gümüşboğa; Altuğ İftar

Fault-tolerant pitch-rate control augmentation system design for asymmetric elevator failures in a combat plane

Kybernetika, Vol. 56 (2020), No. 4, 767–793

Persistent URL: http://dml.cz/dmlcz/148383

KYBERNETIKA — VOLUME *56* (2020), NUMBER 4, PAGES 767–793

FAULT-TOLERANT PITCH-RATE CONTROL AUGMENTATION SYSTEM DESIGN FOR ASYMMETRIC ELEVATOR FAILURES IN A COMBAT PLANE

İlkay Gümüşboğa and Altuğ İftar

Combat planes are designed in a structured relaxed static stability to meet maneuver requirements. These planes are unstable in the longitudinal axis and require continuous active control systems with elevator control. Therefore, failures in the elevator can have vital consequences for flight safety. In this work, the performance of classical control approach against asymmetric elevator failures is investigated and it is shown that this approach is insufficient in the case of such a failure. Then, a fault-tolerant control system is proposed to cope with these failures and it is shown that this controller can successfully deal with such failures. The F-16 aircraft is taken as an example case. A detailed nonlinear dynamic model of this aircraft is presented first. In the F-16 aircraft, the elevator surfaces are in two parts, right and left, and can move independently. Therefore, to obtain a more realistic and difficult failure scenario, it is assumed that the elevator is asymmetrically defective. Two types of failures commonly observed on the elevator surfaces (freezing and floating) are aerodynamically modeled and it is shown that the pitch-rate control augmentation systems in the conventional structure cannot cope with these elevator failures. In order to overcome this problem, a fault-tolerant control system is proposed. It is shown that this controller can successfully cope with the aforementioned failures without any degradation in flight safety.

Keywords: fault-tolerant control, robust control, flight control, control augmentation system, asymmetric elevator failures

Classification: 93B51, 93B36, 93C35, 93D15, 93C95

1. INTRODUCTION

Control surface failures can cause performance degradation in flight control systems, and even system instability leading to serious accidents. Designing a control system for unanticipated failure conditions has been an important and challenging research problem. Control augmentation systems (CASs) are crucial in the aerospace industry because they provide dynamic stability on statically unstable aircraft and undertake specific control functions to reduce the workload of the pilot. These functions include tasks such as precision target tracking, especially on high-performance military aircraft. Control of pitch-rate is the preferred system for a situation that requires precise tracking

DOI: 10.14736/kyb-2020-4-0767

of a target and for critical flight phases such as approach and landing. A pitch-rate CAS design for a healthy F-16 aircraft, in the presence of time-delays in the measurements, has been done by the authors [10]. Furthermore, a detailed aerodynamic model of the F-16 aircraft in the case of asymmetric elevator failures has been obtained in [11]. This modeling study is important because, without such a model, it is not possible to verify the usefulness of the designed controllers. This model was obtained by modifying the full dynamic nonlinear model of the F-16 aircraft, which was obtained in [12].

The longitudinal control system is especially important for combat planes since these planes are unstable in the longitudinal axis. There have been a number of studies of fault-tolerant control (FTC) system design to guarantee longitudinal control system stability and acceptable performance degradation under elevator failures [6,13,17–19]. In some of these studies, a pitch-only thrust vectoring nozzle is used as a redundant control effector such as for the National Aeronautics and Space Administration (NASA) High-Angle-of-Attack Research Vehicle (HARV) [13] and for the F-16 aircraft [18]. [1, 30, 31] introduce the civil aircraft with a redundant actuation system and focuses on modeling of damaged aircraft in a vertical tail loss situation and developing a FTC strategy. On the other hand, [4] uses the control reconfiguration procedure when stuck or floating failures occur on the control surfaces of an unmanned aerial vehicle. In the case of a rudder or aileron jamming failure, [16] proposes an autopilot system that provides flight safety, using the remaining healthy control surfaces. [27] proposes a direct adaptive approach for control of a class of multi-input multi-output nonlinear systems in the presence of uncertain failures of redundant actuators. [24] proposes a novel robust optimal control approach for the attitude stabilization of a flexible spacecraft in the presence of external disturbances.

In the aforementioned literature, failure scenarios are dealt with in a simple way and the assumptions made reduce the realism of the design. In addition, elevator failures are handled symmetrically. The symmetric elevator failures ensure that the effect of the failure is limited to the longitudinal motion of the aircraft. However asymmetric elevator failures, in addition to the negative effect in the longitudinal motion, lead to distortion in the lateral axis. With this distortion, the decoupling between the longitudinal and lateral/directional motion of the aircraft is disrupted. Hence, this condition makes the problem more difficult to solve. Furthermore, most of the literature solves the FTC design problem by including redundant control surfaces and/or actuators. Having redundant control surfaces and/or actuators, which is called as hardware redundancy, however, increase the weight of the aircraft, which is undesirable, especially for combat planes. An alternative approach to hardware redundancy is the so-called aerodynamic redundancy, in which the function of a failed control surface (e. g., elevator) is undertaken by other existing control surfaces (e. g., ailerons and the rudder). This approach provides a weight advantage compared to the hardware redundancy approach.

In the present study, following the aerodynamic redundancy approach, a FTC system is designed which uses the other existing control surfaces to compensate for a failed control surface. Specifically, the case of an asymmetric elevator failure is considered. It is first shown that a controller designed by a classical control approach can not cope with such a failure. Then, a fault-tolerant pitch-rate CAS is designed to cope with asymmetric elevator failures. It is shown that this controller, despite the negative effect

of an asymmetric elevator failure, can continue to execute the desired maneuver without any degradation in flight safety.

In Section 2, the full dynamic nonlinear model of the F-16 aircraft, obtained in [12], is presented and a linear design model is obtained. Then, in Section 3, the modified aerodynamic model, as obtained in [11] for the case of asymmetric elevator failures, is presented and the control surface failures to be considered are detailed. In Section 4, a classical pitch-rate CAS is designed that will work in case of no failure. As it was shown in [11], asymmetric elevator failures cause disturbing effects on both pitch and roll moments. Therefore, in order to make a fair comparison between the conventional pitch-rate CAS and the fault-tolerant CAS, a stability augmentation system (SAS) is also designed for the roll channel in Section 4. In Section 5, a robust FTC system to operate under the asymmetric elevator failures is proposed. By nonlinear flight simulations, it is shown that, although the conventional control systems can not maintain the stability of the aircraft in the case of asymmetric elevator failures, this FTC system continues to maintain the stability and performs the required pitch-rate tracking without any degradation in flight safety. Some concluding remarks are finally given in Section 6. A nomenclature is included in the Appendix.

2. MODELING OF THE F-16 AIRCRAFT

In this section, the complete nonlinear dynamic model of the F-16 aircraft will be presented briefly. The linear design model will then be obtained by a linearization procedure on this nonlinear model. The nonlinear model will also be used to verify the designed controllers in the following sections.

2.1. Nonlinear dynamic model of the F-16 aircraft

A detailed nonlinear dynamic model of the F-16 aircraft has recently been obtained in [12]. The parameters related to the mass and dimensional characteristics of the F-16 aircraft and the details of that model can be found in that reference. In the present subsection, all sub-models that constitute this complete model are summarized briefly.

2.1.1. Control surface actuation model

The control surface (elevator, ailerons, rudder) actuators of the aircraft are modeled as first-order linear lag systems followed by some rate and deflection limits [2, 15, 21]. The inputs to these actuators are the elevator, aileron, and the rudder commands (produced by the pilot or the autopilot), represented by δ_{e_c}, δ_{a_c}, and δ_{r_c}, respectively. The output of each actuator, on the other hand, are the respective control surface deflections, represented by δ_e, δ_a, and δ_r, respectively. The transfer function for the linear lag dynamics is

$$G_{actuator}(s) = \frac{1}{\tau s + 1} \tag{1}$$

where the time constant is $\tau = 49.5 \times 10^{-3}$ seconds. The lag dynamics are the same for all control surfaces, the rate and deflection limits, however, differ for each control surface. These limits, together with the sign convention and the effect produced by each surface, are shown in Table 1 [15].

Control surface	Symbol	Deflection limit (rad)	Rate limit (rad/s)	Positive sign convention	Effect
Elevator	δ_e	± 0.4363	± 1.0472	Trailing edge down	Negative pitching moment
Ailerons	δ_a	± 0.3752	± 1.3963	Right-wing trailing edge down	Negative rolling moment
Rudder	δ_r	± 0.5236	± 2.0944	Trailing edge left	Negative yawing moment, positive rolling moment

Tab. 1. Parameters for the F-16 control surfaces.

2.1.2. Aerodynamic model

The basis of the aerodynamic model is the dataset obtained as a result of wind tunnel tests of the aircraft. In this model, the aerodynamic forces (X, Y, Z) and moments (L, M, N) acting on the aircraft are obtained as:

$$X = C_x \bar{q} S\,;\; Y = C_y \bar{q} S\,;\; Z = C_z \bar{q} S\,;\; L = C_l \bar{q} S b\,;\; M = C_m \bar{q} S \bar{c}\,;\; N = C_n \bar{q} S b \tag{2}$$

where $\bar{q}$, S, b, $\bar{c}$ and denote the dynamic pressure, wing area, wing span, and wing reference chord (all in SI units), respectively. The dimensionless aerodynamic force (C_x, C_y, C_z) and moment (C_l, C_m, C_n) coefficients are expressed as:

$$\begin{aligned}
C_x &= c_x(\alpha, \delta_e) + c_{x_q}(\alpha)\tilde{q} \\
C_y &= c_y(\beta, \delta_a, \delta_r) + c_{y_p}(\alpha)\tilde{p} + c_{y_r}(\alpha)\tilde{r} \\
C_z &= c_z(\alpha, \beta, \delta_e) + c_{z_q}(\alpha)\tilde{q} \\
C_l &= c_l(\alpha, \beta) + c_{l_p}(\alpha)\tilde{p} + c_{l_r}(\alpha)\tilde{r} + c_{l_{\delta_a}}(\alpha, \beta)\delta_a + c_{l_{\delta_r}}(\alpha, \beta)\delta_r \\
C_m &= c_m(\alpha, \delta_e) + c_{m_q}(\alpha)\tilde{q} + (x_{cg_{ref}} - x_{cg})C_z \\
C_n &= c_n(\alpha, \beta) + c_{n_p}(\alpha)\tilde{p} + c_{n_r}(\alpha)\tilde{r} + c_{n_{\delta_a}}(\alpha, \beta)\delta_a + c_{n_{\delta_r}}(\alpha, \beta)\delta_r - (x_{cg_{ref}} - x_{cg})\frac{\bar{c}}{b}C_y
\end{aligned} \tag{3}$$

where $\tilde{p} = \frac{pb}{2V}$, $\tilde{q} = \frac{q\bar{c}}{2V}$, $\tilde{r} = \frac{rb}{2V}$, and the functions $c_x(.)$, $c_{x_q}(.)$, etc. are (multi-) polynomials whose coefficients are determined by a look-up table based on wind tunnel data (see [7,21] for details). Additionally, in these equations, V, α, β, p, and r denote the velocity, the angle of attack (AoA), the sideslip angle, the roll rate and the yaw rate of the aircraft, respectively. Furthermore, x_{cg} is the center-of-gravity location and $x_{cg_{ref}}$ is the reference center-of-gravity location for aerodynamic data, which are both represented as a fraction of $\bar{c}$. In the present study, it is assumed that $x_{cg} = x_{cg_{ref}} = 0.35$. We note that, this corresponds to the relaxed static stability condition, in which the aircraft becomes open-loop unstable in the longitudinal axis.

2.1.3. Propulsion model

The propulsion model calculates the thrust value (T) based on the throttle setting (δ_T) determined by the pilot or the automatic flight control system, the altitude (h), and

the Mach number. This model is constructed using experimental data. In [21, 26], the engine thrust value dataset has been published for the F-16 aircraft.

2.1.4. Gravity model

The gravity model produces different gravitational acceleration values according to the latitude of the geodetic location (λ) on the earth and the altitude of the aircraft (h). This model takes the information of the latitude and the altitude of the aircraft as inputs and calculates the gravitational acceleration, $g(\lambda, h)$, for that location [9, 14]. Since the simulations involve relatively small displacements, in the present study, the latitude, λ, is assumed to be fixed at 30 degrees (chosen arbitrarily, the effect is minimal since, for any given h, the maximum and the minimum of $g(\lambda, h)$ over λ differs only about half a percent; North or South does not make a difference due to symmetry) and the gravity is calculated for the changing altitude, h, which is obtained from the Equations of Motion (EoM) model.

2.1.5. Atmosphere model

The International Standard Atmosphere (ISA) model is taken as the atmospheric model [5]. This model is based on a dataset that describes how the parameters of the atmosphere, such as temperature, pressure, density, and viscosity changes depending on different altitude values.

2.1.6. Equations of motion

The equations of motion consist of kinematic and dynamic equations related to the motion of the aircraft which is caused by the forces (X, Y, Z, T) and the moments (L, M, N) acting on the aircraft. These forces and moments, calculated by the aerodynamic and propulsion models, constitute the inputs of the EoM model. This model consists of twelve nonlinear, coupled, first-order differential equations [8, 15]. The model produces the twelve motion state variables: $V, \alpha, \beta, p, q, r, \phi, \theta, \psi, N_d, E_d$, and h. In here, p, q, r denote the roll, pitch, and yaw rates and ϕ, θ, ψ denote the roll, pitch, and yaw angles, respectively, and N_d and E_d denote the north and east position of the aircraft, respectively.

2.2. Linear Design Model

In this subsection, the linear design model is obtained by linearizing the nonlinear F-16 model presented in the previous subsection. For obtaining the linear time-invariant (LTI) model, a basic numerical linearization procedure is applied [26]. For the LTI model, eight state variables related to longitudinal (V, α, θ, q) and lateral/directional (β, ϕ, p, r) motion are used. The north, east, and yaw state derivatives are a function of other states, but these states themselves are not coupled back into the state equations. Also, the altitude state only enters the aircraft equations through the gravity and the atmosphere models, and in this case, it has negligible coupling to other states. For this reason, these state variables are not represented in the LTI model. As a result, the state and the input vectors to be used in the linearization procedure are taken as follows:

$$\begin{aligned} \bar{x} &= \begin{bmatrix} V & \alpha & \theta & q & \beta & \phi & p & r \end{bmatrix}^T \\ \bar{u} &= \begin{bmatrix} \delta_e & \delta_a & \delta_r \end{bmatrix}^T . \end{aligned} \tag{4}$$

Assuming that all the dynamics, from $\bar{u}$ to $\dot{\bar{x}}$, can be expressed in closed-form as follows:

$$\dot{\bar{x}}(t) = f[\bar{x}(t), \bar{u}(t)] \tag{5}$$

where $\bar{x}(t)$ is the eight-dimensional state vector (t being time), $\bar{u}(t)$ is the three-dimensional control input vector, and f is an eight-dimensional nonlinear function. All the dynamics that affect the system, from the control surface deflections, $\bar{u}(t)$, to the aircraft motion states, $\bar{x}(t)$, are represented by the f function. These dynamics are discussed in detail in Section 2.1. Since the aerodynamic and thrust models are dataset-based models, it is not possible to find analytical expressions for the f function. Therefore, the models created in the MATLAB environment in Section 2.1 are used in the linearization process and the calculations are made numerically. As a general form, the f function is represented as $f = [f_1 \;\; f_2 \;\; ... \;\; f_8]^T$.

A multivariate Taylor-series expansion of the explicit state equations, around an equilibrium point, gives (when higher-order terms are neglected)

$$\Delta\dot{\bar{x}} = \left.\frac{\partial f}{\partial \bar{x}}\right|_{\substack{\bar{x}=x_{trim} \\ \bar{u}=u_{trim}}} \Delta\bar{x} + \left.\frac{\partial f}{\partial \bar{u}}\right|_{\substack{\bar{x}=x_{trim} \\ \bar{u}=u_{trim}}} \Delta\bar{u}. \tag{6}$$

Where partial derivative terms denote Jacobian matrices calculated around trim values and also Δ indicates the deviation from the equilibrium point.

The states and the inputs in the linear model are defined as the deviations of $\bar{x}$ and $\bar{u}$, respectively, around their equilibrium points. In aviation literature, these equilibrium values are called as trim values. The linearized model is obtained using the trim values which are calculated for a specific flight condition: steady wings-level flight, $V = 100\ m/s$, $h = 1000\ m$. The details of the calculation of the trim values can be found in [12]. The trim values for the above-mentioned flight condition are (in SI units):

$$\begin{aligned} x_{trim} &= \begin{bmatrix} 100 & 0.123 & 0.123 & 0 & 0 & 0 & 0 & 0 \end{bmatrix}^T \\ u_{trim} &= \begin{bmatrix} -0.024 & 5 \times 10^{-7} & 7 \times 10^{-7} \end{bmatrix}^T . \end{aligned} \tag{7}$$

Furthermore, the trim value for the throttle setting is calculated as $\delta_T = 11.134$ (throttle setting value is taken as constant at this trim value in all simulations). Thereby, the state and the input vectors for the LTI model are as follows:

$$\begin{aligned} x = \bar{x} - x_{trim} &= \begin{bmatrix} \Delta V & \Delta\alpha & \Delta\theta & \Delta q & \Delta\beta & \Delta\phi & \Delta p & \Delta r \end{bmatrix}^T \\ u = \bar{u} - u_{trim} &= \begin{bmatrix} \Delta\delta_e & \Delta\delta_a & \Delta\delta_r \end{bmatrix}^T . \end{aligned} \tag{8}$$

Resulting state-space representation of the LTI model is:

$$\dot{x} = Ax + Bu \tag{9}$$

where, A and B are the system dynamics and the input matrices, respectively. In order to calculate these matrices, the Jacobian matrices represented in (6) are calculated. The

designed numerical linearization procedure calculates the derivative of the function f to form the corresponding column of the matrix A, perturbing one state variable at a time. After that, in the same way, the linearization procedure calculates the derivative of the function f to form the corresponding column of the matrix B, perturbing one input variable at a time. As a result, the A and B matrices are obtained (in SI units) as follows:

$$A = \begin{bmatrix} -0.022 & -1.395 & -9.828 & -0.672 & 0 & 0 & 0 & 0 \\ -0.002 & -0.582 & 0 & 0.908 & 0 & 0 & 0 & 0 \\ 0 & 0 & 0 & 1 & 0 & 0 & 0 & 0 \\ 3 \times 10^{-7} & 0.324 & 0 & -0.708 & 0 & 0 & 0 & 0 \\ 3 \times 10^{-9} & 0 & 0 & 0 & 0.182 & 0.097 & 0.143 & -0.996 \\ 0 & 0 & 0 & 0 & 0 & 0 & 1 & 0.145 \\ 5 \times 10^{-7} & -4 \times 10^{-6} & 0 & 0 & -19.291 & 0 & -2.047 & 0.716 \\ 3 \times 10^{-7} & -8 \times 10^{-6} & 0 & 0 & 5.364 & 0 & -0.041 & -0.337 \end{bmatrix} \tag{10}$$

$$B = \begin{bmatrix} -1.139 & 0 & 0 \\ -0.072 & 0 & 0 \\ 0 & 0 & 0 \\ -4.301 & 0 & 0 \\ 0 & -0.010 & -0.028 \\ 0 & 0 & 0 \\ 0 & -15.980 & 2.470 \\ 0 & -0.667 & -1.304 \end{bmatrix}. \tag{11}$$

3. ASYMMETRIC ELEVATOR FAILURES

The asymmetric elevator failures considered in this study disrupt the symmetrical movement of the aircraft. Therefore, it causes a loss of control in the pitch axis and a serious disturbance in the roll axis. Note that, the expression for the yaw moment coefficient, C_n, in (3) does not include δ_e. Therefore, the elevator deflection does not have a direct effect on the yaw moment. However, the disturbing roll moment caused by the asymmetric elevator failure also effects the yaw motion due to coupling between the roll and yaw motions through the EoM. Thus, a less significant yaw moment disturbance is also caused, which will be seen in the simulations in the upcoming sections (this effect has also been shown clearly in [11]). The asymmetric elevator failures and the effects of these failures on the aircraft motion have been demonstrated in [11] for the right elevator failures. In that study, the aerodynamic effects of the left and right elevator surfaces were separated and the asymmetric deviation of the elevator was modeled. In this section, this revised model will be presented briefly and the specific failures to be considered will be explained.

3.1. Modeling Aerodynamics of Elevator Failures

The general form of the aerodynamic model, as summarized in Section 2.1.2, is based on three basic control surface deflections (δ_e, δ_a, δ_r). However, to determine the aerodynamic effects of asymmetric failures that may occur on the right and left surfaces of the elevator, the effects of these two elevator surfaces must be decoupled. In order to

separate the contributions of the right and left elevator surface deflections in the aerodynamic model, the technique proposed in [22, 28] is used. In this model, the elevator deflection angle, δ_e, is separated into two deflection angles, δ_{er} and δ_{el}, for the right and left elevators, respectively. The aerodynamic coefficients, C_x, C_z, C_l, and C_m, given in (3), are then modified as follows:

$$\begin{aligned}
C_x &= \frac{1}{2}c_x\left(\alpha,\delta_{er}\right)+\frac{1}{2}c_x\left(\alpha,\delta_{el}\right)+c_{xq}(\alpha)\widetilde{q}\\
C_z &= \frac{1}{2}c_z\left(\alpha,\beta,\delta_{er}\right)+\frac{1}{2}c_z\left(\alpha,\beta,\delta_{el}\right)+c_{zq}(\alpha)\widetilde{q}\\
C_l &= c_l\left(\alpha,\beta\right)+c_{lp}\left(\alpha\right)\widetilde{p}+c_{lr}\left(\alpha\right)\widetilde{r}+c_{l\delta_a}\left(\alpha,\beta\right)\delta_a+c_{l\delta_r}\left(\alpha,\beta\right)\delta_r+\frac{1}{2}L_e(c_z\left(\alpha,\beta,\delta_{el}\right)-c_z\left(\alpha,\beta,\delta_{er}\right))\\
C_m &= \frac{1}{2}c_m\left(\alpha,\delta_{er}\right)+\frac{1}{2}c_m\left(\alpha,\delta_{el}\right)+c_{mq}\left(\alpha\right)\widetilde{q}+(x_{cg_{ref}}-x_{cg})C_z.
\end{aligned} \tag{12}$$

Here, the dimensionless term L_e is given as $L_e=\frac{l_e}{b}$, where l_e is the distance from the x-axis to the aerodynamic center of any one of the elevator surfaces, which is taken as $1.69\ m$, based on the data presented in [28]. The coefficients C_x, C_z, and C_m determine the forces and moments acting on the x-z plane. The contribution of the elevator surfaces to these forces and moments is expressed through the functions c_x, c_z, and c_m. These functions are expressed as multi-polynomials of their arguments, whose coefficients are determined by look-up tables based on wind tunnel data [7, 21]. Although the wind tunnel data is taken for a healthy aircraft, where the right and left elevator surfaces move identically, clearly the effect of each of the two elevator surfaces in the x-z plane is equal [22,28]. Therefore, in (12), the effect of each elevator surface is simply expressed as half of the effect of the two elevator surfaces when they move together. The asymmetric movement of the elevator surfaces also cause a roll moment. This moment is due to the different force contribution of each surface in the z-direction, which is expressed by the c_z function. Therefore, to represent this effect, the term $\frac{1}{2}L_e(c_z\left(\alpha,\beta,\delta_{el}\right)-c_z\left(\alpha,\beta,\delta_{er}\right))$ is added to the C_l equation as shown in (12). Since the elevator surfaces does not have a direct effect on the lateral force or the yaw moment, C_y and C_n coefficients in (3) are not changed. More details of this model are presented and its effects are analyzed in [11].

3.2. Control Surface Failures

In this study, *freezing* (or *lock-in-place*) and *floating* failures commonly encountered in aircraft control surfaces are examined [3]. In many aircraft, the elevator surface is one piece. However, F-16 aircraft has two independent elevator surfaces, controlled by two different actuators. Thus, there is a possibility of a failure in one of these independent surfaces. As mentioned earlier, the asymmetric failure of the elevator, besides causing a loss of control in the pitch moment, also causes a roll moment disturbance and, hence, is a more difficult scenario to control compared to an identical failure in both elevator surfaces. If both of the elevator surfaces fail in the same way, the disturbing effect of the failure would only affect the longitudinal states of the aircraft. Therefore, in the present study, an asymmetric elevator failure scenario is considered. It is assumed that the failure occurs only in the right elevator. When one of these two failures (freezing or floating) occurs, rather than the actual elevator command, δ_{e_c}, a modified signal, δ_{er_f},

is assumed to enter to the elevator model, presented in Section 2.1.1.

In the freezing failure, the control surface command becomes locked in its last position before the failure occurs. Therefore,

$$\delta_{er_f}(t) = \delta_{e_c}(t_f), \quad \forall t \geq t_f \tag{13}$$

where t_f is the time of failure.

In the floating failure, the control link that drives the control surface breaks. This corresponds to the zero hinge moment state and the control surface deflects in accordance with the air flow passing over it. Therefore, when a floating failure occurs, it is assumed that the right elevator deflects according to the AoA of the aircraft. Therefore, in this case:

$$\delta_{er_f}(t) = -0.5\alpha(t), \quad \forall t \geq t_f. \tag{14}$$

The models obtained herein and the detailed examination of the effects of these failures on the motion of the aircraft have been previously demonstrated in [11].

4. CONVENTIONAL PITCH-RATE CAS AND ROLL-AXIS SAS

In this section, the conventional pitch-rate CAS and roll-axis SAS structures commonly found in the literature will be examined.

4.1. Conventional Pitch-Rate CAS

The general structure of a conventional pitch-rate CAS system is represented in Figure 1 [20,26]. In this figure, q and α, which denote the pitch-rate and the AoA of the aircraft, respectively, constitute the measurements form the aircraft and the elevator command, δ_{e_c}, constitutes the control input. Since the design of the control system is based on the linear model, the deviations of q, α, and δ_{e_c} (Δq, $\Delta\alpha$, and $\Delta\delta_{e_c}$) around the trim values (q_{trim}, α_{trim}, and $\delta_{e_{c_{trim}}}$) are also shown in this figure. Furthermore, $\Delta q_r = q_r - q_{trim}$, where q_r denotes the pitch-rate reference signal.

Since this control system is effective on the longitudinal dynamics of the aircraft, as the aircraft model, the longitudinal sub-model from the complete LTI model obtained in (9) – (11) is selected as follows (in SI units):

$$\begin{bmatrix} \Delta\dot{V} \\ \Delta\dot{\alpha} \\ \Delta\dot{\theta} \\ \Delta\dot{q} \end{bmatrix} = \begin{bmatrix} -0.022 & -1.395 & -9.828 & -0.672 \\ -0.002 & -0.582 & 0 & 0.908 \\ 0 & 0 & 0 & 1 \\ 3 \times 10^{-7} & 0.324 & 0 & -0.708 \end{bmatrix} \begin{bmatrix} \Delta V \\ \Delta\alpha \\ \Delta\theta \\ \Delta q \end{bmatrix} + \begin{bmatrix} -1.139 \\ -0.072 \\ 0 \\ -4.301 \end{bmatrix} [\Delta\delta_e] \tag{15}$$

$$y_{lon} = \begin{bmatrix} \Delta q \\ \Delta\alpha \end{bmatrix} = \begin{bmatrix} 0 & 0 & 0 & 1 \\ 0 & 1 & 0 & 0 \end{bmatrix} \begin{bmatrix} \Delta V \\ \Delta\alpha \\ \Delta\theta \\ \Delta q \end{bmatrix} \tag{16}$$

where y_{lon} denotes the measurement for the longitudinal model. The eigenvalues of the dynamics matrix are $\{-0.1256 \pm 0.1507j,\ -1.1950,\ 0.1351\}$. The complex-conjugate eigenvalues shown here are associated with the short period modes. The last two real eigenvalues are associated with the phugoid mode and there is instability in this mode.

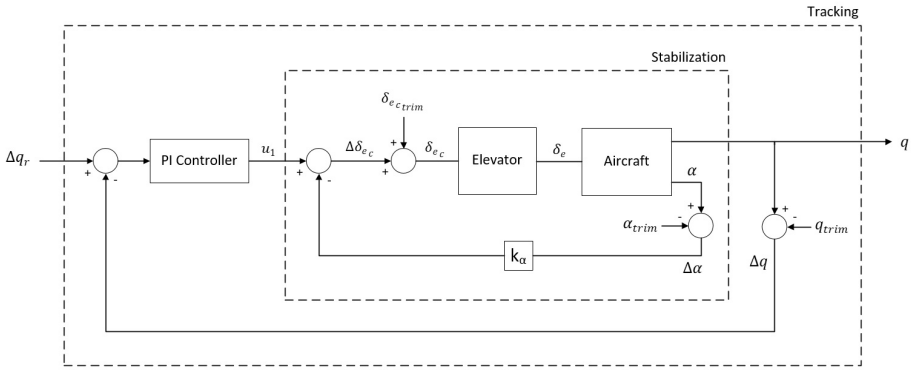

Fig. 1. Conventional pitch-rate CAS.

The control input to this model is the elevator surface deflection angle, δ_e, which is the output of the elevator actuator. The transfer function for the actuator dynamics (the transfer function from δ_{e_c} to δ_e) is obtained as the negative of the linear part of the actuator model:

$$P(s) = \frac{-20.2}{s + 20.2}. \tag{17}$$

The negative sign is due to the fact that the positive elevator deflection causes a negative pitching moment.

The control system shown in Figure 1 obviously consists of two nested feedback loops. In the inner loop, the $\Delta\alpha$ signal is fed back, with a static controller, k_α, in the feedback path. In the outer loop, the Δq is fed back through a proportional-integral (PI) controller in the forward path, which has the transfer function:

$$C_{PI}(s) = k_{prop} + \frac{k_i}{s}. \tag{18}$$

In this control system, the internal loop provides the dynamic stability of the F-16 longitudinal motion model of the statically unstable aircraft, while the outer loop performs the reference pitch-rate tracking.

The design procedure will be to close the inner loop, then design the proportional-integral (PI) controller in Simulink by using the PID Tuner tool (here the D coefficient is set to zero initially, since the conventional control is PI only, which is because having overshoots is acceptable and the speed of response is the important parameter) to yield a satisfactory transient response. First of all, in the inner loop, $\Delta\alpha$ feedback is used to stabilize the system. Considering the inner loop, the k_α gain is determined by the root-locus method as $k_\alpha = 0.08$. When the inner loop is closed with this feedback gain, the eigenvalues of the system (before the outer loop is closed) are obtained as $\{-20.2105,$ $-0.6434 \pm 0.1628j,\ -0.0069 \pm 0.0290j\}$. It is obvious that all eigenvalues have been moved into the left half complex plane and thus the stability of the system has been

ensured. After the inner loop is closed with the $\Delta\alpha$ feedback, proportional and integral coefficients are determined using the *PID Tuner* tool in Simulink software as follows:

$$k_{prop} = 1 \;\; and \;\; k_i = 0.75. \tag{19}$$

This controller is used in the feedback system shown in Figure 1 and the step response is obtained as shown in Figure 2. It is evident that the controller stabilizes the system and has a good transient response.

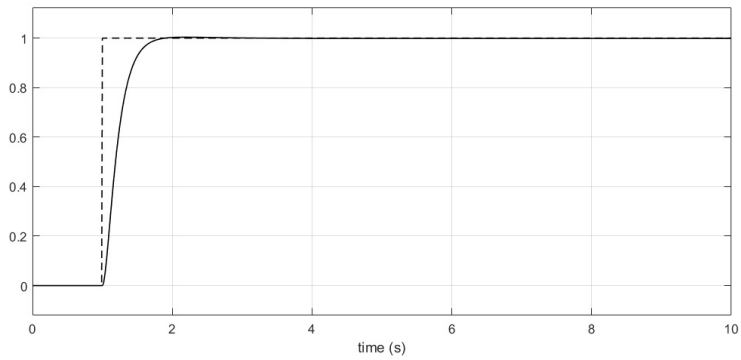

Fig. 2. The step response of the conventional pitch-rate CAS (linear simulation). Dashed line: Δq_r, rad/s. Solid line:Δq, rad/s.

4.2. Roll-Axis SAS

The most basic augmentation system for the lateral dynamics is shown in Figure 3. To improve the roll out characteristics of an aircraft, roll-rate feedback is used. The augmentation system is also known as roll damper and it helps to increase the roll mode stability of an aircraft [25].

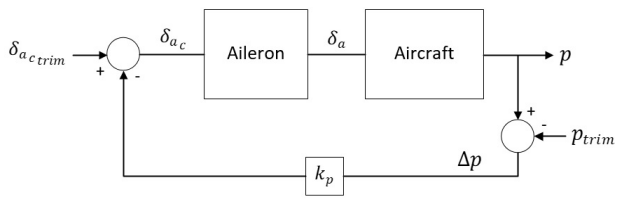

Fig. 3. Roll-axis SAS.

Since this control system is effective on the lateral/directional dynamics of the aircraft, as the aircraft model, the lateral/directional sub-model from the complete LTI

model obtained in (9) – (11) is selected as follows (in SI units):

$$\begin{bmatrix} \dot{\Delta\beta} \\ \dot{\Delta\phi} \\ \dot{\Delta p} \\ \dot{\Delta r} \end{bmatrix} = \begin{bmatrix} 0.182 & 0.097 & 0.143 & -0.996 \\ 0 & 0 & 1 & 0.145 \\ -19.291 & 0 & -2.047 & 0.716 \\ 5.364 & 0 & -0.041 & -0.337 \end{bmatrix} \begin{bmatrix} \Delta\beta \\ \Delta\phi \\ \Delta p \\ \Delta r \end{bmatrix} + \begin{bmatrix} -0.010 \\ 0 \\ -15.980 \\ -0.667 \end{bmatrix} [\Delta\delta_a] \tag{20}$$

$$y_{lat} = \Delta p = \begin{bmatrix} 0 & 0 & 1 & 0 \end{bmatrix} \begin{bmatrix} \Delta\beta \\ \Delta\phi \\ \Delta p \\ \Delta r \end{bmatrix} \tag{21}$$

where y_{lat} denotes the measurement for the lateral/directional model. The eigenvalues of the dynamics matrix are $\{-0.2013 \pm 2.7585j,\ -1.7926,\ -0.0067\}$. The complex-conjugate eigenvalues correspond to the dutch-roll mode, the real eigenvalue near the origin corresponds to the spiral mode, and the real eigenvalue that is away from the origin corresponds to the roll mode.

The control input to this model is the aileron surface deflection angle, δ_a, which is the output of the aileron actuator. The linear model used for the aileron actuator is the same as for the elevator actuator and is given by (17).

The roll rate feedback gain, k_p, is determined by the root-locus method. Here, increasing of k_p improves roll stability. However, a large gain may reduce robustness and may cause a violation of control surface actuator's deflection and rate limits. For this reason, a feedback gain of $k_p = 0.1$ is chosen, which puts the roll mode at $s = -3.68$.

4.3. Verification of Pitch-Rate CAS and Roll-Axis SAS by Nonlinear Flight Simulations

In this subsection, in order to test the performance of the controllers designed using the linear models, flight simulations are made using the complete nonlinear F-16 model described in Section 2.1. In these simulations, the aircraft is required to follow a certain pitch-rate reference signal, which is shown in Figure 4. This pitch-rate reference signal is chosen to perform an agile altitude reduction maneuver within the limits of the maneuvering capability of the aircraft.

In the remaining of this paper, the control system structure including pitch-rate CAS and roll-axis SAS is called as the *classical controller*. The performance of this classical controller under various conditions is investigated separately in the following subsubsections. Firstly, the healthy condition is examined. After that, the performance of the classical controller is examined in the case of two different asymmetric elevator failures.

4.3.1. Healthy aircraft

In this subsubsection, the healthy aircraft is examined. This simulation shows how the aircraft, which is required to follow the pitch-rate reference signal shown in Figure 4, moves with the designed controllers in the absence of any failure or disturbance. When the nonlinear flight simulation is run in this way, the states of the aircraft are obtained as in Figure 5 (solid lines). Additionally, the control surface commands, deflections, and deflection rates produced within this simulation are shown in Figure 6 (solid lines).

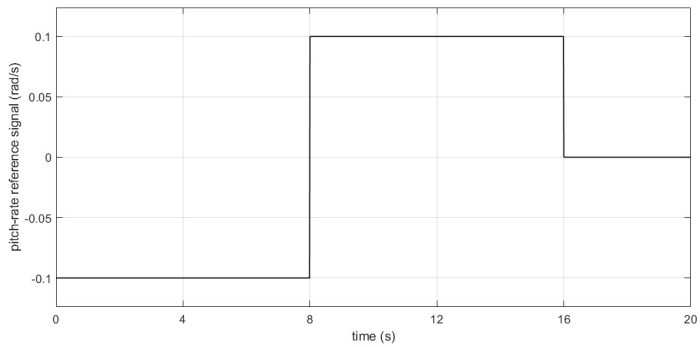

Fig. 4. Pitch-rate reference signal.

Since the control structure designed in this simulation does not control the rudder, the rudder deflection is kept constant at the trim value during the entire simulation.

After the simulation starts, the aircraft moves to the dive and after the eighth second, it starts to nose upwards according to the pitch-rate reference given in Figure 4. The pitch-rate state of the aircraft indicates that the pitch-rate CAS works well and performs the tracking function very quickly. On the other hand, the aircraft continued its symmetrical flight because there is no disturbance in the lateral/directional axis. Therefore, the lateral/directional states remained almost zero. The control surface deflections and rates shown in Figure 6 (solid lines) show that the designed control system operates within the deflection and rate limits shown in Table 1.

4.3.2. Freezing failure

In this subsubsection, the condition of freezing failure is examined. Right after the eighth second of the twenty-seconds nonlinear simulation, when the control system moves the elevator to apply the reverse pitch-rate command, to follow the pitch-rate reference given in Figure 4, the right elevator is stuck in its extreme position. In this example, the right elevator is jammed at -0.1981 radians after the 8.17th second.

When the nonlinear flight simulation is run for the above conditions, the states of the aircraft are obtained as in Figure 5 (dashed lines). Additionally, the control surface commands, deflections, and deflection rates produced within this simulation are shown in Figure 6 (dashed lines).

It is clear that the conventional control system cannot handle the failure. The roll rate has consistently increased and has reached a high magnitude that will challenge the structural boundaries of the aircraft. The aircraft speedily turned around the body x-axis and dived to the ground before the end of the simulation period. Additionally, pitch-rate tracking has also failed. Figure 6c (dashed line) shows that the right elevator is jammed after the 8th second. The control surface deflections and rates shown in Figure 6 (dashed lines) show that the designed control system operates within the deflection and rate limits shown in Table 1.

4.3.3. Floating failure

In this subsubsection, the condition of floating failure is examined. In the eighth second of the twenty-seconds nonlinear simulation, when the control system moves the elevator to apply the reverse pitch-rate command, to follow the pitch-rate reference given in Figure 4, the right elevator starts to float.

When the nonlinear flight simulation is run for the above conditions, the states of the aircraft are obtained as in Figure 5 (dotted lines). Additionally, the control surface commands, deflections, and deflection rates produced within this simulation are shown in Figure 6 (dotted lines).

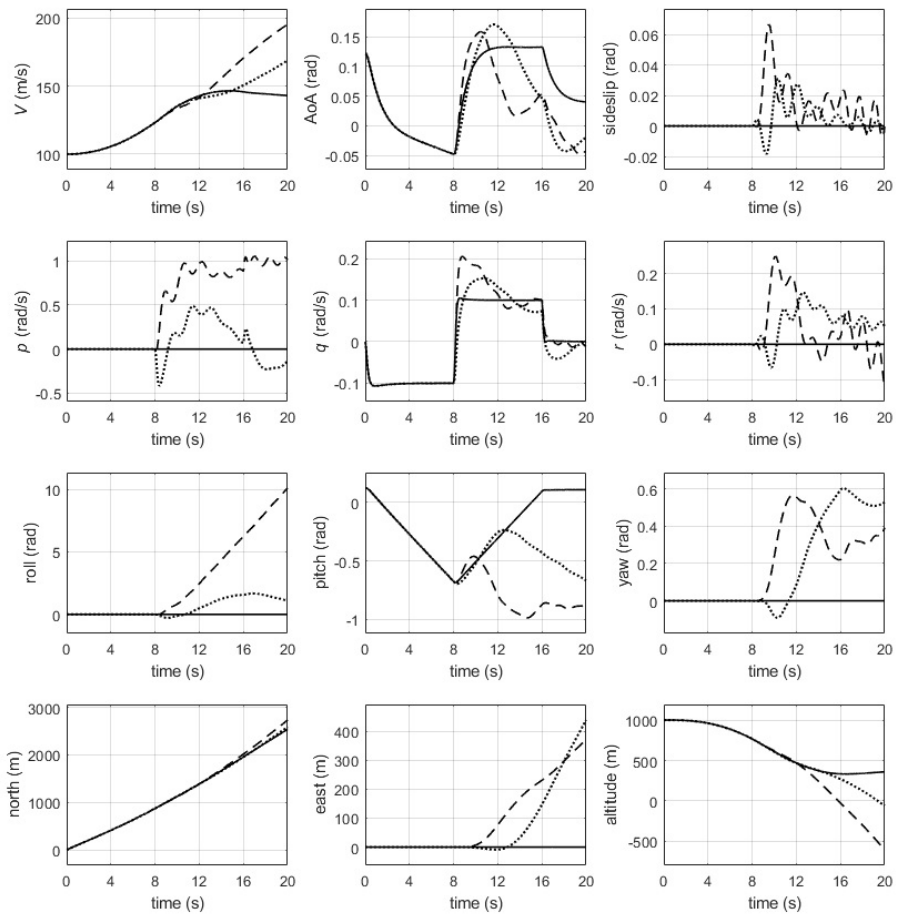

Fig. 5. The states of the F-16 aircraft (classical controller nonlinear simulation solid line: healthy condition; dashed line: freezing failure; dotted line: floating failure).

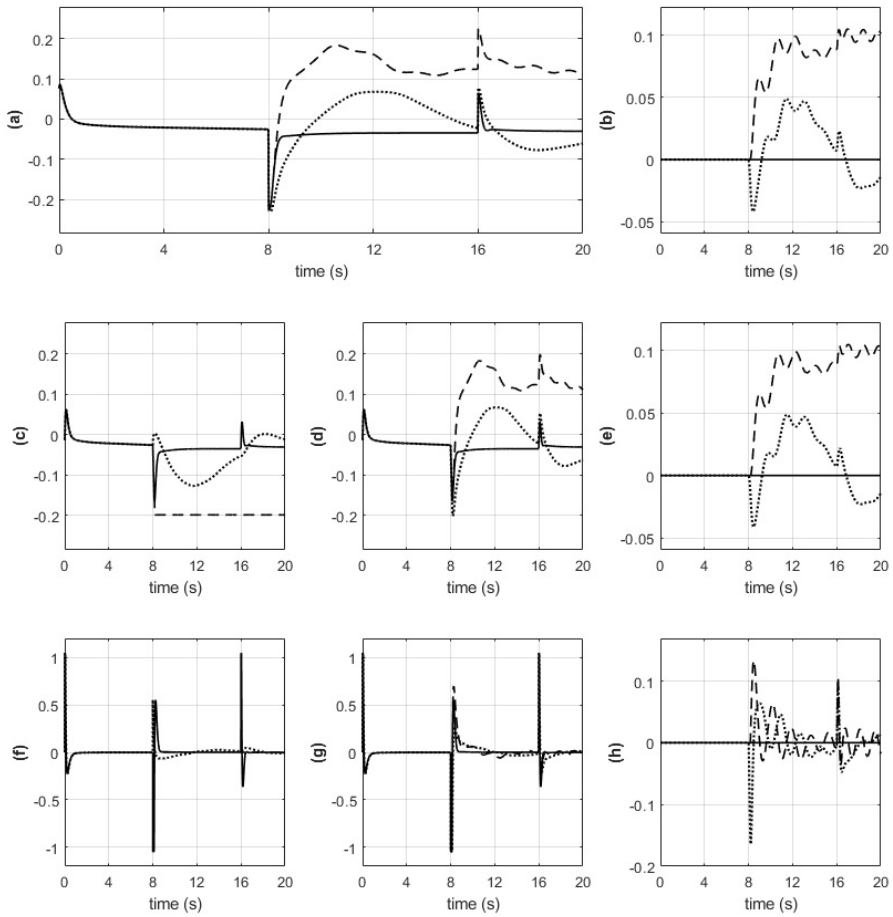

Fig. 6. The control surface commands, deflections, and deflection rates (classical controller nonlinear simulation solid line: healthy condition; dashed line: freezing failure; dotted line: floating failure). (a) Elevator command, rad. (b) Aileron command, rad. (c-d) Right and left elevator deflections respectively, rad. (e) Aileron deflection, rad. (f-g): Right and left elevator deflection rates respectively, rad/s. (h) Aileron deflection rate, rad/s.

It is clear that the conventional control system cannot handle this failure either. The roll rate has consistently increased and has reached a high magnitude that will challenge the structural boundaries of the aircraft. The aircraft speedily turned around the body x-axis and dived to the ground before the end of the simulation period. Additionally, pitch-rate tracking has also failed. As shown in Figure 6c (dotted line), the right elevator

floats after the 8th second. The control surface deflections and rates shown in Figure 6 (dotted lines) show that the designed control system operates within the deflection and rate limits shown in Table 1.

As a result, all these simulations have shown that the designed classical controller works well in healthy conditions. However, it cannot cope with asymmetric failures on the elevator. In the following section, a fault-tolerant control system will be designed to deal with these failures. Furthermore, the performance of these designed control system structures will be compared.

5. FAULT-TOLERANT PITCH-RATE CAS

In this section, the design of the robust controller that will work in the faulty condition is undertaken. The proposed control system structure is designed as a nested loop structure based on the conventional pitch-rate CAS described in Figure 1. The conventional structure is revised to have an H_∞ controller in the inner loop [23]. The H_∞ controller structure is chosen since it is one of the most effective design strategies when robustness against both unknown disturbances and modeling uncertainties is required [29]. In this way, it is aimed to design a robust controller that can maintain the dynamic stability of the aircraft in the case of control surface failures. This control structure has two objectives. The first is that the controller eliminates the disturbing effect of the failures and continues the flight of the aircraft in a safe way. The second is that the aircraft follows a certain reference pitch-rate command despite the disturbing effect of the failures. The proposed control structure is shown in Figure 7.

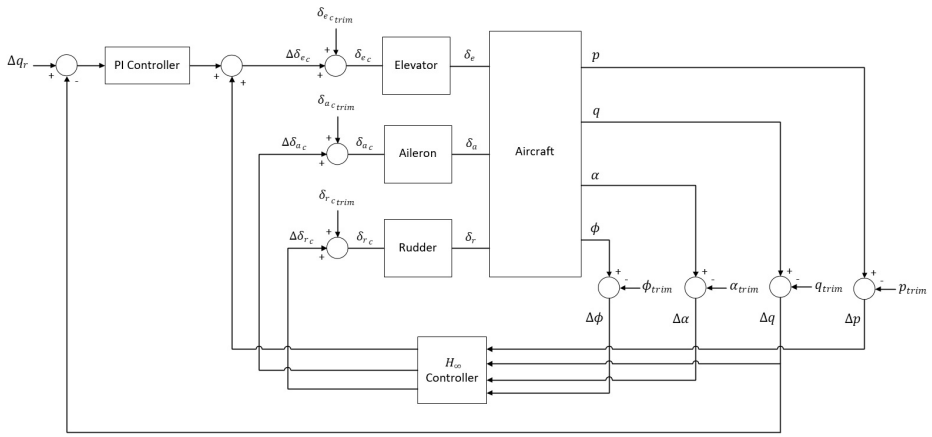

Fig. 7. The control structure of fault-tolerant pitch-rate CAS.

5.1. Design Procedures of the Fault-Tolerant Pitch-Rate CAS

In this subsection, the design of the control system shown in Figure 7 is presented. Firstly, the design of the inner loop is explained. Then, the design of the outer loop is explained.

5.1.1. Design of the inner loop

The H_∞ control approach is used in the design of the inner loop robust controller. Details of the design procedure for this method are described in [29]. This section describes the problem representation used in the design of this controller. Firstly, an extended F-16 model is derived so that it can be used to solve the elevator failure scenario. The state-space representation of the extended F-16 model is as follows:

$$\begin{aligned} \dot{x}_{ext} &= A_{ext}x_{ext} + B_1 w + B_2 u_c \\ z &= C_1 x_{ext} + D_{11} w + D_{12} u_c \\ y &= C_2 x_{ext} + D_{21} w + D_{22} u_c \end{aligned} \tag{22}$$

In this model, the vector x_{ext} consists of control surface deviations in addition to the current states, $x_{ext} = [\Delta V\ \Delta\alpha\ \Delta\theta\ \Delta q\ \Delta\beta\ \Delta\phi\ \Delta p\ \Delta r\ \Delta\delta_e\ \Delta\delta_a\ \Delta\delta_r]^T$ and u_c consists of control commands, $u_c = [\Delta\delta_{e_c}\ \Delta\delta_{a_c}\ \Delta\delta_{r_c}]^T$. For this control problem, it is assumed that the roll and pitch rates, as well as the AoA and the roll angle, are available for measurement. Therefore, the measurement output vector is chosen as $y = [\Delta p\ \Delta q\ \Delta\alpha\ \Delta\phi]^T$.

The most important vectors in this problem representation are the disturbance input, w, and the performance output, z, vectors. The H_∞ control method minimizes the effects of w disturbance on the z outputs. Therefore, these vectors should be selected in accordance with the elevator failure problem. It is known that asymmetric elevator failure leads to disturbances in pitch and roll moment. In addition, since the symmetry of the aircraft is disturbed, different forces and moments can also occur with coupling effects. Therefore, the vector w has been chosen as moment and force disturbances, $w = [\delta L\ \delta M\ \delta N\ \delta X\ \delta Y\ \delta Z]^T$. Since it is aimed to minimize the effect of these disturbances on the roll and pitch rates, as well as on the roll angle, the deviations of these variables from their trim values must be chosen as a part of the z vector. Furthermore, since the control surface deflections and their rates must satisfy certain limits, the deviations of these variables from their trim values must also be chosen as a part of the z vector. Therefore, we choose $z = Q[\Delta p\ \Delta q\ \Delta\phi\ \Delta\delta_e\ \Delta\delta_a\ \Delta\delta_r\ \Delta\dot{\delta}_e\ \Delta\dot{\delta}_a\ \Delta\dot{\delta}_r]^T$, where Q is a constant diagonal weight matrix with positive diagonal elements, which are all taken as unity in the present application. The matrices for this extended system are obtained as follows:

$$\begin{gathered} A_{ext} = \begin{bmatrix} A & B \\ 0_{3\times 8} & -20.2I_3 \end{bmatrix}, B_1 = \begin{bmatrix} \widetilde{B}_1 \\ 0_{3\times 6} \end{bmatrix}, B_2 = \begin{bmatrix} 0_{8\times 3} \\ -20.2I_3 \end{bmatrix}, C_1 = Q \begin{bmatrix} \widetilde{C}_1 & 0_{3\times 3} \\ 0_{3\times 8} & I_3 \\ 0_{3\times 8} & -20.2I_3 \end{bmatrix} \\ D_{11} = 0_{9\times 6}, D_{12} = Q \begin{bmatrix} 0_{3\times 3} \\ I_3 \\ -20.2I_3 \end{bmatrix}, C_2 = \begin{bmatrix} \widetilde{C}_2 & 0_{4\times 3} \end{bmatrix}, D_{21} = 0_{4\times 6}, D_{22} = 0_{4\times 3} \end{gathered} \tag{23}$$

where, subindexed 0 and I denotes zero and identity matrices of indicated dimensions, respectively. Furthermore, A and B are given in (10) and (11), respectively,

and (in SI units):

$$\widetilde{B}_1 = \begin{bmatrix} 0 & 0 & 0 & 1\times10^{-4} & 0 & 1\times10^{-5} \\ 0 & 0 & 0 & -1\times10^{-6} & 0 & 8\times10^{-6} \\ 0 & 0 & 0 & 0 & 0 & 0 \\ 0 & 1\times10^{-5} & 0 & 0 & 0 & 0 \\ 0 & 0 & 0 & 0 & -1\times10^{-6} & 0 \\ 0 & 0 & 0 & 0 & 0 & 0 \\ 8\times10^{-5} & 0 & 1\times10^{-6} & 0 & 0 & 0 \\ 1\times10^{-6} & 0 & 1\times10^{-5} & 0 & 0 & 0 \end{bmatrix}, \tag{24}$$

$$\widetilde{C}_1 = \begin{bmatrix} 0 & 0 & 0 & 0 & 0 & 0 & 1 & 0 \\ 0 & 0 & 0 & 1 & 0 & 0 & 0 & 0 \\ 0 & 0 & 0 & 0 & 0 & 1 & 0 & 0 \end{bmatrix}, \text{ and } \widetilde{C}_2 = \begin{bmatrix} 0 & 0 & 0 & 0 & 0 & 0 & 1 & 0 \\ 0 & 0 & 0 & 1 & 0 & 0 & 0 & 0 \\ 0 & 1 & 0 & 0 & 0 & 0 & 0 & 0 \\ 0 & 0 & 0 & 0 & 0 & 1 & 0 & 0 \end{bmatrix}$$

Using this problem representation, a robust controller is designed in MATLAB environment using the H_∞ control design tool. The state-space realization of the robust controller designed is as follows:

$$\begin{aligned} \dot{\hat{x}} &= \hat{A}\hat{x} + \hat{B}y \\ u_c &= \hat{C}\hat{x} + \hat{D}y \end{aligned} \tag{25}$$

where $\hat{x}$ is the state vector for the controller and (in SI units):

$$\hat{A} = \begin{bmatrix} -0.022 & 52.987 & -9.828 & 6.984 & 0 & 0.003 & -0.005 & 0 & -1.140 & -3\times10^{-15} & 0 \\ -0.002 & -1.092 & 0 & 0.736 & 0 & 6\times10^{-6} & 1\times10^{-5} & 0 & -0.072 & 7\times10^{-17} & 0 \\ 0 & -0.834 & 6\times10^{-11} & 0.690 & 0 & 2\times10^{-5} & 4\times10^{-5} & 0 & -1\times10^{-20} & 1\times10^{-16} & 0 \\ 2\times10^{-7} & 0.095 & 0 & -0.939 & 0 & 1\times10^{-6} & 2\times10^{-6} & 0 & -4.301 & 1\times10^{-16} & 0 \\ 3\times10^{-9} & -3\times10^{-6} & 0 & -5\times10^{-7} & 0.182 & 0.081 & 0.254 & -0.996 & -5\times10^{-17} & -0.010 & -0.028 \\ 0 & 9\times10^{-6} & 0 & 1\times10^{-6} & 0 & -0.872 & 0.514 & 0.145 & 2\times10^{-16} & -5\times10^{-22} & 0 \\ 5\times10^{-7} & 1\times10^{-5} & 0 & 2\times10^{-6} & -19.291 & -0.486 & -5.292 & 0.716 & 1\times10^{-15} & -15.980 & 2.469 \\ 3\times10^{-7} & -3\times10^{-6} & 0 & 9\times10^{-7} & 5.364 & 0.085 & -0.024 & -0.337 & -8\times10^{-18} & -0.667 & -1.304 \\ -1\times10^{-4} & 0.1462 & 4\times10^{-4} & 0.710 & 4\times10^{-5} & -2\times10^{-5} & -8\times10^{-6} & -4\times10^{-6} & -2.481 & 3\times10^{-5} & -4\times10^{-6} \\ 7\times10^{-7} & -8\times10^{-6} & -4\times10^{-8} & -1\times10^{-5} & -33.445 & 12.954 & 6.508 & 5.509 & 3\times10^{-5} & -26.499 & 4.394 \\ -3\times10^{-9} & -2\times10^{-6} & -7\times10^{-7} & 1\times10^{-6} & 8.259 & -2.265 & -1.168 & -0.887 & -4\times10^{-6} & 4.394 & -1.3527 \end{bmatrix}$$

$$\hat{B} = \begin{bmatrix} 1.534 & -2\times10^{3} & -1\times10^{4} & 0.896 \\ -0.004 & 57.778 & 129.159 & -0.002 \\ -0.013 & 104.164 & 211.074 & -0.007 \\ -8\times10^{-4} & 77.677 & 57.778 & -3\times10^{-4} \\ -37.403 & 1\times10^{-4} & 7\times10^{-4} & 5.387 \\ 162.994 & -3\times10^{-4} & -0.002 & 292.588 \\ 1\times10^{3} & -8\times10^{-4} & -0.004 & 162.994 \\ -5.838 & -3\times10^{-4} & -0.001 & 28.411 \\ 0 & 0 & 0 & 0 \\ 0 & 0 & 0 & 0 \\ 0 & 0 & 0 & 0 \end{bmatrix}$$

$$\hat{C} = \begin{bmatrix} 3\times10^{-8} & -3\times10^{-5} & -8\times10^{-8} & -1\times10^{-4} & -8\times10^{-9} & 3\times10^{-9} & 2\times10^{-9} & 9\times10^{-10} & -0.004 & -6\times10^{-9} & 9\times10^{-10} \\ -2\times10^{-10} & 2\times10^{-9} & 9\times10^{-12} & 3\times10^{-9} & 0.007 & -0.003 & -0.002 & -0.001 & -6\times10^{-9} & 0.001 & -9\times10^{-4} \\ 7\times10^{-13} & 4\times10^{-10} & 1\times10^{-10} & -2\times10^{-10} & -0.002 & 4\times10^{-4} & 2\times10^{-4} & 2\times10^{-4} & 9\times10^{-10} & -8\times10^{-4} & -0.004 \end{bmatrix}$$

$$\hat{D} = \ 0_{3\times4}.$$

5.1.2. Design of the outer loop

After the robust controller for the inner loop is designed, the structure in Figure 7 is implemented in the Simulink software. The coefficients for the PI controller are then determined by using the *PID Tuner* tool in Simulink as follows:

$$k_{prop} = 1.5 \ \ and \ \ k_i = 1.1. \tag{26}$$

5.2. Verification of the Designed Control Structure by Nonlinear Flight Simulations

In this subsection, in order to test the performance of the controllers designed using the linear models, flight simulations are made using the complete nonlinear F-16 model described in Section 2.1. In these simulations, the aircraft is required to follow a certain pitch-rate reference signal, which is shown in Figure 4, while the asymmetric failures occur in the right elevator surface.

5.2.1. Healthy condition

In this subsubsection, the healthy aircraft is examined. This simulation shows how the aircraft, which is required to follow the pitch-rate reference signal shown in Figure 4, moves with the designed controller in the absence of any failure or disturbance. When the nonlinear flight simulation is run in this way, the states of the aircraft are obtained as in Figure 8 (solid lines). Additionally, the control surface commands, deflections, and deflection rates produced within this simulation are shown in Figure 9 (solid lines).

After the simulation starts, the aircraft moves to the dive and after the eighth second, it starts to nose upwards according to the pitch-rate reference given in Figure 4. The pitch-rate state of the aircraft indicates that the fault-tolerant pitch-rate CAS works well and performs the tracking function very quickly. On the other hand, the aircraft continued its symmetrical flight because there is no disturbance in the lateral/directional axis. Therefore, the lateral/directional states remained almost zero. Additionally, the control surface deflections and rates shown in Figure 9 (solid lines) show that the designed control system operates within the deflection and rate limits shown in Table 1.

5.2.2. Freezing failure

In this subsubsection, the condition of freezing failure is examined. Right after the eighth second of the twenty-seconds nonlinear simulation, when the control system moves the elevator to apply the reverse pitch-rate command, to follow the pitch-rate reference given in Figure 4, the right elevator is stuck in its extreme position. In this example, the right elevator is jammed at -0.1981 radians after the 8.17th second.

When the nonlinear flight simulation is run for the above conditions, the states of the aircraft are obtained as in Figure 8 (dashed lines). Additionally, the control surface commands, deflections, and deflection rates produced within this simulation are shown in Figure 9 (dashed lines).

A significant roll moment is produced on the aircraft, due to the asymmetric failure of the elevator right after the 8th second. However, with the fault-tolerant control system, the disturbing effect of this roll moment is rejected very quickly. Besides, the other states of the longitudinal motion vary in accordance with the executed pitch-rate maneuver, while the states for the lateral/directional motion change at very small magnitudes.

Figure 9d (dashed line) shows that the right elevator is jammed after the 8th second. The control surface deflections and rates shown in Figure 9 (dashed lines) show that the designed control system operates within the deflection and rate limits shown in Table 1.

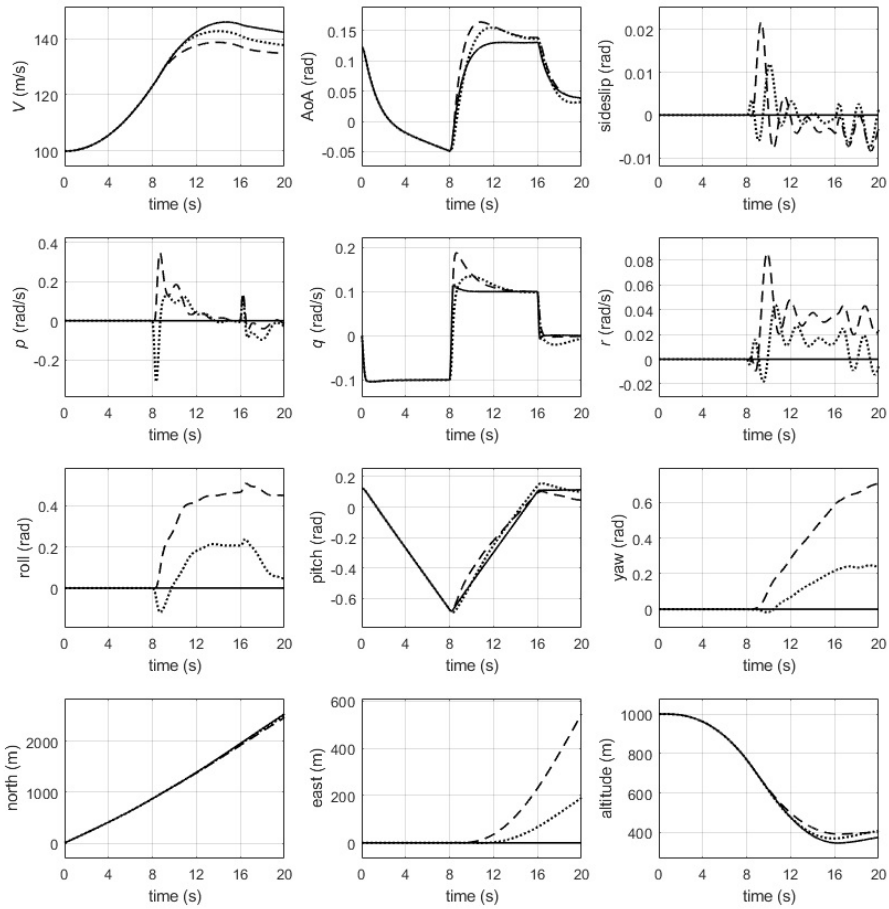

Fig. 8. The states of the F-16 aircraft (fault-tolerant controller nonlinear simulation solid line: healthy condition; dashed line: freezing failure; dotted line: floating failure).

5.2.3. Floating failure

In this subsubsection, the condition of floating failure is examined. In the eighth second of the twenty-seconds nonlinear simulation, when the control system moves the elevator to apply the reverse pitch-rate command, to follow the pitch-rate reference given in Figure 4, the right elevator starts to float. When the nonlinear flight simulation is run for the above conditions, the states of the aircraft are obtained as in Figure 8 (dotted lines). Additionally, the control surface commands, deflections, and deflection rates produced within this simulation are shown in Figure 9 (dotted lines). In this case too, a significant roll moment is produced on the aircraft, due to the asymmetric failure

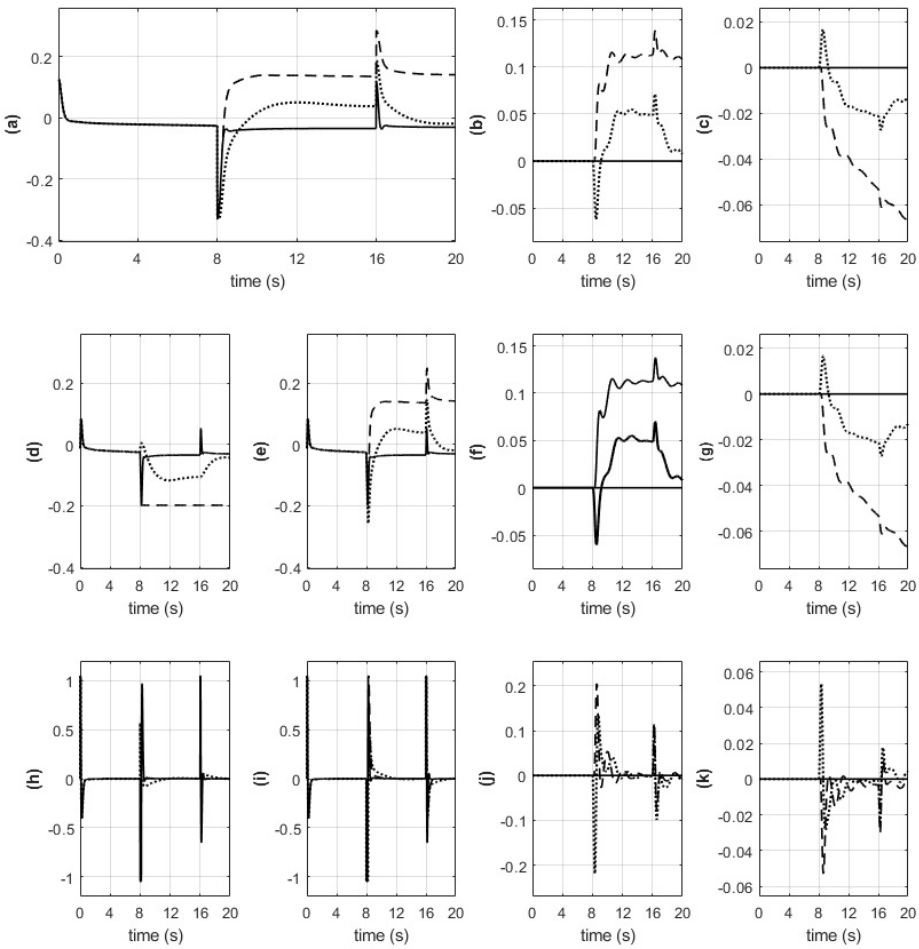

Fig. 9. The control surface commands, deflections, and deflection rates (fault-tolerant controller nonlinear simulation solid line: healthy condition; dashed line: freezing failure; dotted line: floating failure). (a-b-c) Elevator, aileron, and rudder commands respectively, rad. (d-e-f-g) Right and left elevator, aileron, and rudder deflections respectively, rad. (h-i-j-k) Right-and left elevator, aileron, and rudder deflection rates, respectively, rad/s.

of the elevator at the 8th second. However, the fault-tolerant control system rejects the disturbing effect of this roll moment very quickly. Besides, the other states of the longitudinal motion vary in accordance with the executed pitch-rate maneuver, while the states for the lateral/directional motion change at very small magnitudes. Figure 9d

(dotted line) shows that the right elevator floats after the 8th second. The control surface deflections and rates shown in Figure 9 (dotted lines) show that the designed control system operates within the deflection and rate limits shown in Table 1.

5.3. Comparison of Classical and Fault-Tolerant Controllers

In Section 4, the classical controller (the pitch-rate CAS and roll-axis SAS) was designed that will work in case of no failure. It has been shown in Section 4.3.1 that this classical

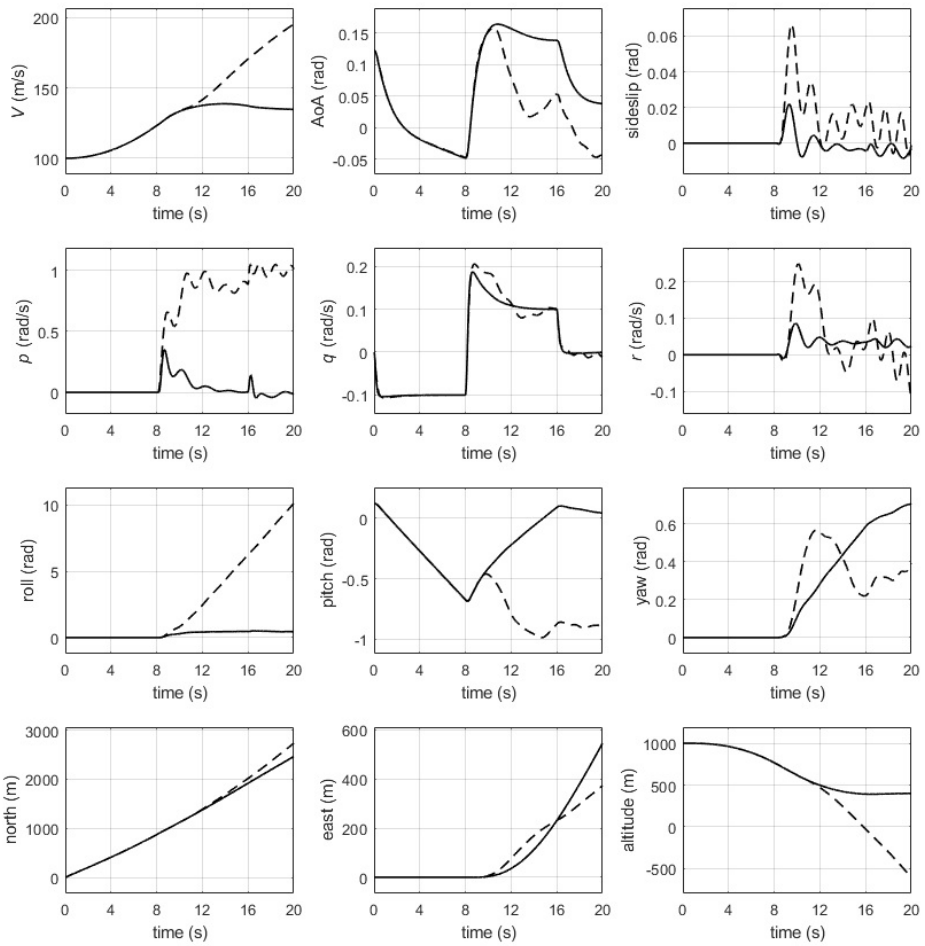

Fig. 10. The states of the F-16 aircraft in the case of freezing failure (comparison of the fault-tolerant controller and the classical controller nonlinear simulation solid line: fault-tolerant controller; dashed line: classical controller).

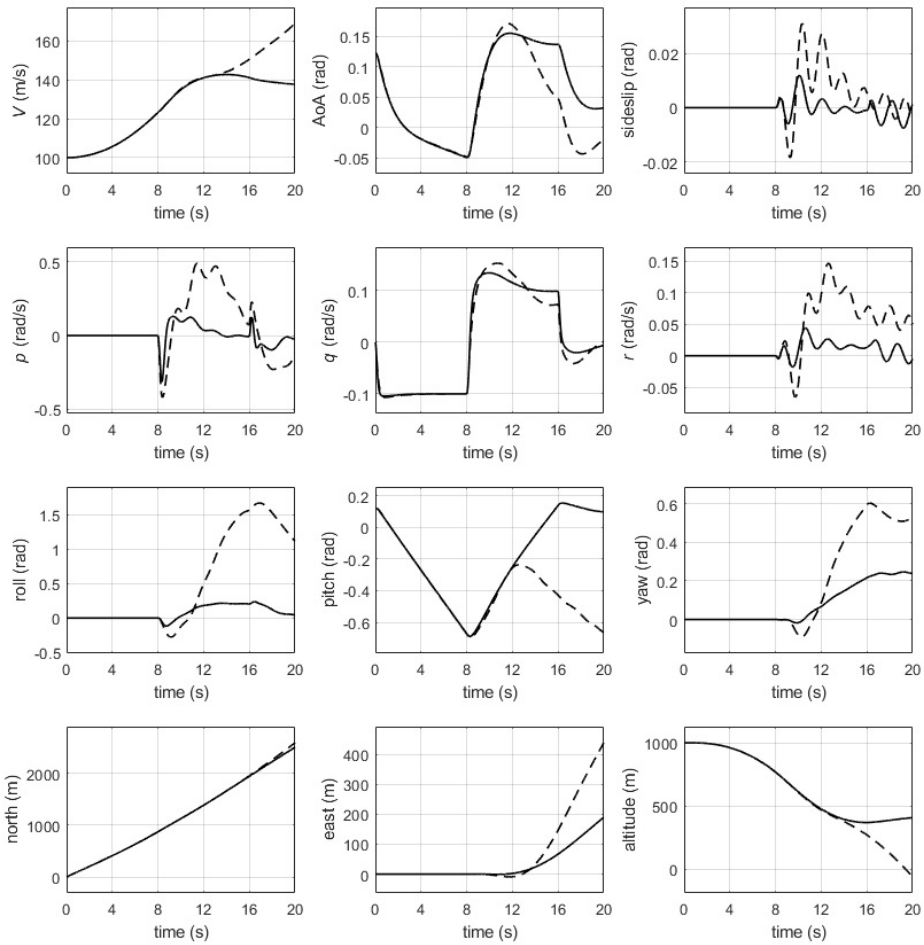

Fig. 11. The states of the F-16 aircraft in the case of floating failure (comparison of the fault-tolerant controller and the classical controller nonlinear simulation solid line: fault-tolerant controller; dashed line: classical controller).

controller produces a very good response (in terms of stability and pitch-rate tracking) in case of no failures. It has, however, also been shown in Sections 4.3.2 and 4.3.3 that this controller cannot cope with the asymmetric elevator failures.

In the present section, as the main purpose of the current work, the design of a fault-tolerant pitch-rate CAS has been undertaken. The nested loop structure shown in Figure 7 has been proposed for this purpose. In this structure, the H_∞ method is used to design the inner loop. This inner loop acts like a stability augmentation system

to robustly stabilize the system despite disturbances caused by the asymmetric elevator failures. The outer loop, on the other hand, includes the PI controller to achieve pitch-rate tracking. It has been shown in Section 5.2 that, this controller produces a good response in both non-faulty and faulty conditions.

In this subsection, in order to compare the performance of the two controllers, states of the aircraft under classical and proposed controllers are reproduced in Figure 10, in the case of freezing failure, and in Figure 11, in the case of floating failure. Under the classical controller, following the occurrence of the failure, the aircraft rolls around its body x-axis and crashes to the ground. Under the proposed fault-tolerant controller, however, the roll motion is stabilized quickly and the required pitch maneuver is executed as required, despite the failure. In particular, the altitude changes according to the desired dive motion and the aircraft can continue to fly safely. In both responses, due to the roll disturbance, the yaw state is also disturbed. As a result of this, the airplane sways to east. This disturbance, however, can easily be corrected by the pilot or the autopilot when the fault-tolerant controller is active (under the classical controller, due to violent roll motion and loss of AoA, it would not be possible to control the plane). Since the yaw state is related to the route to which the aircraft should go, it is not controlled by the classical or the fault-tolerant CAS.

6. CONCLUSIONS

The asymmetric elevator failures are fatal malfunctions that disrupt flight safety. In this study, it has been shown that the classical control systems in the literature cannot cope with these failures. Therewith, the primary purpose of the present study has been to develop a fault-tolerant controller design approach such that the aircraft continues to fly safely and can complete its mission in the case of such a failure. As discussed in Section 5.3, this proposed fault-tolerant control system has been shown to cope with the asymmetric elevator failures while the conventional approach has failed.

This study has provided a general approach to the fault-tolerant control design against control surface failures on an aircraft. Asymmetric elevator failure is selected as a case study. The method proposed in this study can also be applied to aileron and rudder failures. This, however, may require separate control of each elevator and each aileron surface, since aileron failures may be compensated by separate control of left and right elevator surfaces and rudder failures can be compensated to some degree by using each elevator and each aileron surface separately.

ACKNOWLEDGEMENT

The authors received financial support from the Turkish Aerospace Industries Inc. through grant TM3021 for the research of this article.

APPENDIX: NOMENCLATURE

$\alpha,\ \beta$	Angle of attack and sideslip angle, respectively (rad)
$\delta_e,\ \delta_a,\ \delta_r$	Elevator, aileron and rudder deflections, respectively (rad)
$\delta_{e_c},\ \delta_{a_c},\ \delta_{r_c}$	Elevator, aileron and rudder deflection commands, respectively (rad)
$\delta_{er},\ \delta_{el}$	Right and left elevator surface deflections, respectively (rad)
δ_{er_f}	Failed right elevator deflection command (rad)
δ_T	Throttle setting, [0-100]
λ	Latitude of the geodetic location (rad)
τ	Time constant (s)
$\phi,\ \theta,\ \psi$	Euler angles: roll, pitch, and yaw, respectively (rad)
a_{trim}	Trim value of a vector (or variable) a
$\dot{a}$	Derivative of a vector (or variable) a with respect to time
A^T	Transpose of a matrix A
b	Wing span (m)
$\bar{c}$	Wing reference chord (m)
$C_x,\ C_y,\ C_z$	x-, y-, and z-axis force coefficients, respectively
$C_l,\ C_m,\ C_n$	Rolling, pitching, and yawing moment coefficients, respectively
h	Altitude (m)
l_e	Distance from the x-axis to the aerodynamic center of the elevator (m)
$L,\ M,\ N$	Rolling, pitching, and yawing moments, respectively (N.m)
$N_d,\ E_d$	North and east geographic positions of the aircraft, respectively (m)
$p,\ q,\ r$	Roll, pitch, and yaw rates, respectively (rad/s)
q_r	Pitch-rate reference signal (rad/s)
$\bar{q}$	Dynamic pressure (N/m^2)
S	Wing area (m^2)
t_f	Time of failure (s)
T	Thrust (N)
V	True velocity (m/s)
x_{cg}	Center-of-gravity location
$x_{cg_{ref}}$	Reference center-of-gravity location for aerodynamic data
$X,\ Y,\ Z$	Total X-, Y-, and Z-axis forces, respectively (N)
$0_{m\times n}$	$m \times n$-dimensional zero matrix
I_n	$n \times n$-dimensional identity matrix

(Received August 8, 2019)

REFERENCES

[1] H. Alwi and C. Edwards: Fault detection and fault-tolerant control of a civil aircraft using a sliding-mode-based scheme. IEEE Trans. Control Systems Technol. *16* (2008), 499–510. DOI:10.1109/tcst.2007.906311

[2] J. H. Blakelock: Automatic Control of Aircraft and Missiles. John Wiley and Sons, 1991.

[3] J. D. Boskovic and K. M. Raman: A decentralized fault-tolerant control system for accommodation of failures in higher-order flight control actuators. IEEE Trans. Control Systems Technol. *18* (2009), 5, 1103–1115. DOI:10.1109/tcst.2009.2033805

[4] F. Caliskan and C. Hajiyev: Active fault-tolerant control of UAV dynamics against sensor-actuator failures. J. Aerospace Engrg. *29* (2016), 4, 04016012. DOI:10.1061/(asce)as.1943-5525.0000579

[5] M. Cavcar: The International Standard Atmosphere (ISA). Technical Report, Anadolu University, 2000.

[6] B. C. Chang, H. Kwatny, C. Belcastro, and C. Belcastro: Aircraft loss-of-control accident prevention: Switching control of the GTM aircraft with elevator jam failures. In: Proc. AIAA Guidance, Navigation and Control Conference, Honolulu 2008, pp. 1–15. DOI:10.2514/6.2008-6507

[7] A. Eugene: Global nonlinear parametric modeling with application to F-16 aerodynamics. In: Proc. American Control Conference, Philadelphia 1998, pp. 997–1001.

[8] B. Etkin and L. D. Reid: Dynamics of Flight: Stability and Control. Wiley, New York 1996.

[9] P. D. Groves: Principles of GNSS, Inertial, and Multisensor Integrated Navigation Systems. Artech House, 2013.

[10] İ. Gümüşboğa and A. İftar: Pitch-rate control augmentation system design for delayed measurements. In: Proc. 6th International Conference on Control, Decision and Information Technologies, Paris 2019. DOI:10.1109/codit.2019.8820480

[11] İ. Gümüşboğa and A. İftar: Modeling of asymmetrical elevator failures in the F-16 aircraft. In: Proc. AIAA SciTech Forum and Exposition, San Diego 2019. DOI:10.2514/6.2019-0111

[12] İ. Gümüşboğa and A. İftar: Aircraft trim analysis by particle swarm optimization. J. Aeronaut Space Technol. *12* (2019), 2, 185–196.

[13] R. A. Hess and C. McLean: Development of a Design Methodology for Reconfigurable Flight Control Systems. NASA Technical Report Server (NTRS), 2000. DOI:10.2514/6.2000-890

[14] B. Hofmann-Wellenhof, H. Lichtenegger, and J. Collins: Global Positioning System: Theory and Practice. Springer Science and Business Media, 2012.

[15] Y. Huo: Model of F-16 Fighter Aircraft. Technical Report, University of Southern California, 2007.

[16] C. Kasnakoglu and U. Kaynak: Automatic recovery and autonomous navigation of disabled aircraft after control surface actuator jam. In: Proc. AIAA Guidance, Navigation, and Control Conference, Toronto 2010.

[17] C. Lin and L. Chun-Te: Failure detection and adaptive compensation for fault tolerable flight control systems. IEEE Trans. Industr. Inform. *3* (2007), 322–331. DOI:10.1109/tii.2007.913064

[18] B. Lu and W. Fen: Switching-based fault-tolerant control for an F-16 aircraft with thrust vectoring. In: Proc. 48th IEEE Conference on Decision and Control, Shanghai 2009, pp. 322–331. DOI:10.1109/cdc.2009.5400385

[19] P. Lu, E. J. Kampen, C. Visser, and Q. Chu: Aircraft fault-tolerant trajectory control using incremental nonlinear dynamic inversion. Control Engingrg. Practice *57* (2016), 126–141. DOI:10.1016/j.conengprac.2016.09.010

[20] R. C. Nelson: Flight Stability and Automatic Control. WCB/McGraw Hill, New York 1998.

[21] L. T. Nguyen, M. E. Ogburn, W. P. Gilbert, K. S. Kibler, P. W. Brown, and P. L. Deal: Simulation Study of Stall/post-stall Characteristics of a Fighter Airplane with Relaxed Static Stability. Technical Report, NASA-TP-1538, NASA Langley Research Center, Hampton 1979. DOI:10.4271/790604

[22] D. T. Ocana, S. Hyo-Sang, and A. Tsourdos: Development of a nonlinear reconfigurable F-16 model and flight control systems using multilayer adaptive neural networks. IFAC-PapersOnLine *48* (2015), 138–143. DOI:10.1016/j.ifacol.2015.08.073

[23] I. R. Petersen: Robust H^{∞} control of an uncertain system via a stable decentralized output feedback controller. Kybernetika *45* (2009), 1, 101–120.

[24] C. Pukdeboon: Robust optimal PID controller design for attitude stabilization of flexible spacecraft. Kybernetika *54* (2018), 5, 1049–1070. DOI:10.14736/kyb-2018-5-1049

[25] J. Roskam: Airplane Flight Dynamics and Automatic Flight Controls. DARcorporation, 1998.

[26] B. L. Stevens, F. L. Lewis, and E. N. Johnson: Aircraft Control and Simulation: Dynamics, Controls Design, and Autonomous Systems. John Wiley and Sons, 2015.

[27] X. Tang, T. Gang, and M. J. Suresh: Adaptive actuator failure compensation for nonlinear MIMO systems with an aircraft control application. Automatica *43* (2007), 1869–1883. DOI:10.1016/j.automatica.2007.03.019

[28] S. Thomas, G. K. Harry, and C. Bor-Chin: Nonlinear reconfiguration for asymmetric failures in a six degree-of-freedom F-16. In: Proc. American Control Conference, Boston 2004, pp. 1823–1828. DOI:10.23919/acc.2004.1386845

[29] K. Zhou, J. C. Doyle, and K. Glover: Robust and Optimal Control. Prentice Hall, New Jersey 1996.

[30] J. Wang, S. Wang, X. Wang, C. Shi, and M. M. Tomovic: Active fault tolerant control for vertical tail damaged aircraft with dissimilar redundant actuation system. Chinese J. Aeronautics *29* (2016), 1313–1325. DOI:10.1016/j.cja.2016.08.009

[31] X. Wang, S. Wang, Z. Yang, and C. Zhang: Active fault-tolerant control strategy of large civil aircraft under elevator failures. Chinese J. Aeronautics *28* (2015), 1658–1666. DOI:10.1016/j.cja.2015.10.001

İlkay Gümüşboğa, Department of Avionics, Eskişehir Technical University, Eskişehir 26555. Turkey.
e-mail: ilkaygumusboga@eskisehir.edu.tr

Altuğ İftar, Department of Electrical and Electronics Engineering, Eskişehir Technical University, Eskişehir 26555. Turkey.
e-mail: aiftar@eskisehir.edu.tr